ORIGINAL ARTICLE

Quantitative Elemental Analysis Using Whole Spectral Information (with GA and MLR Methods) of Proton Induced Prompt Gamma-Rays Simulated Using Geant4 Toolkit

Fereshte Saheli [1*], Naser Vosoughi [1], Zafar Riazi [2], Fatemeh S. Rasouli [3], Alireza Jowkar [2]

[1] *Department of Energy Engineering, Sharif University of Technology, Tehran, Iran*

[2] *Physics and Accelerator Research School, Nuclear Science and Technology Research Institute, Tehran, Iran*

[3] *Department of Physics, K.N. Toosi University of Technology, Tehran, Iran*

*Corresponding Author: Fereshte Saheli
Email: fereshte.saheli@gmail.com

Received: 27 June 2022 / Accepted: 09 November 2022

Abstract

Purpose: Online determination of the elemental composition of tissues near the Bragg peak is a challenge in proton therapy related studies. In the present work, an analysis method based on the whole spectral information is presented for the quantitative determination of the elemental composition (weight %) of an irradiated target from its emitted Prompt Gamma (PG) spectrum.

Materials and Methods: To address this issue, four test phantoms with different weights (%) of ^{12}C, ^{16}O, ^{20}Ca, and ^{14}N elements were considered. The simulated PG spectra were recorded using 3 × 3 inch NaI detectors. A library consisting of the spectra of single-element phantoms as well as the spectra of test-irradiated phantoms was produced for 30, 70, and 150 MeV incident protons using the Geant4 Monte Carlo toolkit. The elemental analysis was performed using the information of the whole spectrum by applying two methods, including the well-known Genetic Algorithm (GA) and Multiple Linear Regression (MLR).

Results: The results show that the proposed method estimates the oxygen concentration accurately. Furthermore, the estimated weights of other elements, with both methods, agree well with nominal values in each test phantom, for the considered energies.

Conclusion: The proposed quantitative elemental analysis of proton-bombarded phantoms using their induced PG spectrum is expected to be beneficial in treatment planning and treatment verification studies.

Keywords: Proton Therapy; Prompt Gamma-Ray Spectrum; Whole Spectrum Analysis; Genetic Algorithm; Multiple Linear Regression.

DOI: https://doi.org/10.18502/fbt.v10i1.11515

1. Introduction

The sharp peak of the end of the range, known as the Bragg peak, offered by proton beam therapy allows tumors to be exposed to higher doses while minimizing the energy deposited in healthy surrounding tissues [1]. However, the full potential advantage of this method could only be achieved by the precise prediction of the Bragg peak position in treatment planning systems and its online verification [2]. The online monitoring of dose distribution is essential to avoid the destructive effect of deviations of the real treatment from the predicted dose distribution [3, 4]. The detection of gamma rays produced in proton therapy is one of the best candidates to this aim. The gamma monitoring can be performed by either the β+ emitters or prompt photons [5-8]. While real-time monitoring needs complex Post processing in Positron Emission Tomography (PET) [9], Prompt Gamma (PG) produced by non-elastic nuclear interactions in target and incident protons within a few Pico-seconds, can be used for online monitoring in proton therapy due to their immediate production and relatively larger yield [10].

The pioneering study of Stichelbaut and Jongen [11] suggested the possibility of using PGs for monitoring the particle range in hadron therapy. After that, Min *et al.* in 2006 [12] and Testa *et al.* in 2008 [13] preliminary detected PG spectra experimentally. In recently published studies, Polf *et al.* [14-16] and Verburg *et al.* [17, 18] found a correlation between the delivered Spread-Out Bragg Peak (SOBP) dose distribution and the characteristic PG-ray production in the presence of tissues with an unknown composition.

The potential of using PG emission as a method to acquire information about the irradiated target has been investigated in proton therapy [16, 19]. Their proposed method is based on specific gamma lines in the recorded gamma-ray spectrum of the phantom. According to the best of our knowledge, there is no attempt at an accurate quantitative elemental analysis of whole spectral information of PG spectra generated in proton therapy.

It has been previously demonstrated that using whole information of gamma-ray spectrum would lead to more accurate results in the gamma-ray spectroscopy applications like PG neutron activation analysis [20], radioisotope identification [21, 22], and environmental radioactivity [23].

In the present study, a quantitative elemental analysis is presented to evaluate the elements' weight (%) in some test phantoms, using their whole information of PG spectra. In the analysis algorithm, two conventional methods with a whole spectrum approach, the Genetic Algorithm (GA), and the Multiple Linear Regression (MLR) were applied.

2. Materials and Methods

2.1. Monte Carlo Simulation

In the present study, the Geant 4.10.03 toolkit [24] was applied to simulate single-element and multi-element phantoms for evaluating the feasibility of PG spectroscopy in the accurate elemental analysis of tissues. To consider different shallow and deep-seated tumors, different incident proton beams of 30 MeV, 70 MeV, and 150 MeV were used in simulations. The approximate ranges of protons in phantoms of this study are: 0.6 cm for 30 MeV, 3 cm for 70 MeV, and 11 cm for 150 MeV. The NaI scintillation detector was applied to record the high-energy PG-rays. The primary support reason to choose NaI detector is its good detection efficiency for high-energy PG-rays. The arrangement of the spectroscopy system is shown in Figure 1. The target was considered as a cuboid of 2 × 2 × 2 cm^3 for 30 MeV, 6 × 2 × 2 cm^3 for 70 MeV, and 20 × 2 × 2 cm^3 for 150 MeV beams. As can be seen in part (a) of Figure 1, the detection system consists of two 3 × 3 inch NaI(Tl) crystals as

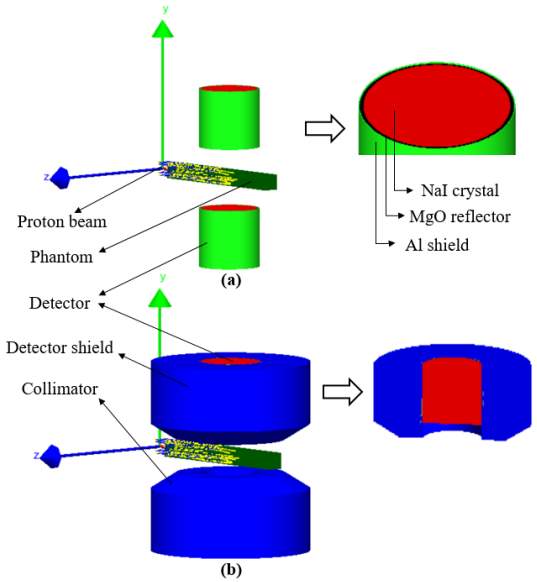

Figure 1. A schematic view of the geometry of the detection system used in this study without (a) and with (b) lead shield and collimator

the main scintillator, MgO as a reflector layer (0.2 cm thick), and an aluminum shield (0.05 cm thick). To decrease the required time for Monte Carlo simulations, we used two identical detectors in opposite sides. According to the previous studies [14, 15], the detectors were located at a 90 angle with respect to the direction of the proton beam's central axis as shown in Figure1. The detectors were also positioned in the Bragg peak region to record the maximum yield of produced PG-rays. A planar source with dimensions of 2cm × 2cm was used in simulations for mentioned proton energies. As shown in Figure 1, the detector shield and collimator were considered to investigate their roles in analysis results by removing the majority of the unwanted radiations named background. Undesired gamma rays are the counts produced in the depth of tissue, except in the Bragg peak region. These counts may be recorded in each channel of the spectra. For example, Although the 4.44 MeV gamma rays originated from the Bragg peak region are the desired gamma rays that include beneficial information, the 4.44 MeV gamma rays originated from out of the Bragg peak region are undesired and therefore should be shielded and collimated to prevent overestimating mass concentration of each element.

A cylindrical lead shield with a thickness of 6.2 cm along with a semi-quartic collimator [25, 26] presented in Figure 1b was used in Monte Carlo simulations. The energy cut-off was set equal to a range of 100 μm for proton, gamma, electron, and positron in different phantoms in the simulations.

In this work, our analysis method was applied to the following different scenarios:

•The reliability of the proposed analysis method was investigated in quantitative analysis of different phantoms. To do this, the 30 MeV protons as the source and four phantoms presented in Table 1 as the targets were considered in Monte Carlo simulations. Oxygen, Carbon, Nitrogen, and Calcium display a similar trend in their gamma-ray emission as a function of proton beam energy. For each element, gamma-ray emission rises sharply at low proton energies reaching a maximum between 25 MeV and 35 MeV [14]. So, the 30 MeV proton energy produces the maximum gamma fluence and it is an appropriate energy for feasibility studies. Also, the proton energy is adjusted the through treatment plan in each clinical case.

• To evaluate the applicability of the proposed method in analyzing an irradiated phantom with different proton energies, phantom 3 of Table 1 was irradiated by 30, 70, and 150 MeV protons in different simulations.

• The collimator role in improving the analysis results was investigated by analyzing the obtained detector spectra related to the 70 MeV proton energy and phantom 3 of Table 1.

Table 1. Density and elemental composition of the test phantoms

		Elemental composition (% mass)			
	ρ (gcm^{-3})	C	O	N	Ca
Phantom1	0.95	66.75	31.45	1.80	0
Phantom2	0.26	11.86	84.63	3.51	0
Phantom3	1.52	27.10	50.60	4.70	17.60
Phantom4	1.05	16.12	80.04	3.84	0

For all incident proton energies, the simulations were carried out in two steps. In the first step, the phantom material was chosen to be ^{12}C, ^{16}O, ^{20}Ca, and ^{14}N single elements and the resulting PG spectra were recorded in the detectors. The libraries generated from gamma-ray spectra of these given elements were established to be used as a reference to find the weight (%) of that element inside an unknown target. In the second step, four test phantoms were simulated.

Since the hydrogen concentration is mapped to zero in this study, we couldn't entitle the defined phantoms as human tissues. Therefore, these are only defined phantoms though they can be extended to other tissues with estimated hydrogen concentration in unknown phantoms through any biological methods such as the method presented in Ref. [27] and scale other elements' concentration. This is not a shortcoming of our work, in fact, the interaction between proton and hydrogen does not produce any characteristic prompt gamma rays. So, the analysis method based on the prompt gamma spectrum cannot estimate the hydrogen level.

The resolution of the detector was also taken into account in simulations by convolving the Geant4 results with the Full Width at Half Maximum (FWHM) of the NaI detector. The FWHM of NaI detector shows a nonlinear response versus energy and can be calculated by Equation 1:

$$FWHM = a + b\sqrt{E + cE^2} \quad (1)$$

Where E is the incident gamma-ray energy and constant parameters a, b, and c depend on the detector type, size, and front-end electronics. In this work, these parameters were taken from ref. [28] for high energy PG-rays recorded in a 3 × 3 inch NaI detector with the following values:

$a = -0.00789\ MeV$;

$b = 0.06769\ MeV^{\frac{1}{2}}$;

$c = 0.21159\ MeV^{-1}$

Once the gamma-ray spectra were produced for single and compound phantoms using the Monte Carlo approach, the weight (%) of elements was calculated by applying the GA and MLR analysis methods in each test phantom.

2.2. Analysis Methods

Whole Spectrum Analysis (WSA) is one of the well-known elemental analysis methods. It has been previously introduced to overcome the disadvantages of the peak analysis method in gamma-ray spectroscopy [20, 22]. The entire gamma-ray spectrum, including both the photopeaks and the Compton continuum is taken into account in the WSA method [22]. In this method, it is assumed that the detector spectrum is a linear combination of contributing fundamental library spectra in an unknown sample, as in Equation 2 [29, 30]:

$$N + \varepsilon = Rx \qquad (2)$$

Here, the vector N is the recorded detector gamma-ray spectrum related to the unknown sample; ε is the statistical error related to the detector spectrum; R is the response matrix of the detector in which the columns are the fundamental library spectra; and x is the contribution of the sample components.

In the present study, the WSA method is applied for the elemental analysis of PG-ray spectra induced in proton therapy. This approach is implemented using two optimization methods: the MLR and GA method.

The analytical optimization MLR method has frequently been used for the analysis of gamma-ray spectra in the literature [21, 29, 31]. It makes use of all the available constituent of library spectra to fit an unknown PG-ray spectrum using linear regression [22, 29]. As there are four constituent library spectra (^{12}C, ^{16}O, ^{20}Ca, and ^{14}N) considered in the current work, the MLR is applied with four library spectra.

The GA method is an artificial intelligence optimization technique [32-35] that has been successfully applied for analyzing complex gamma-ray spectra with the WSA method [21, 36]. For gamma-ray spectrum analysis, the GA method is applied to minimize both the Mean Absolute Error (MAE) and the Root Mean Square Error (RMSE) as presented in Refs. [30, 36]. The standard deviation of the estimated values using the GA method is also calculated as shown in Equation 3 [21, 31].

$$\sigma(x_j) = \frac{||N - N_{est}||_2}{\sqrt{n-m} \times ||R_j - \bar{R}_j||_2},\ j = 1, \dots, m \qquad (3)$$

Here, N is the detector spectrum; N_{est} is the estimated spectrum; $\sigma(x_j)$ is the standard deviation of the estimated values; R_j is the jth column of the response matrix with a dimension of n; and $\bar{R}_j$ is the mean of the jth column of the response matrix.

The developed algorithm was applied for analyzing the simulated PG-ray spectra using the obtained response matrices and the results are presented in the next section.

Verification of the simulations is of high importance and the straightforward method is to compare the various simulated gamma lines to the experimental ones. We have compared all of the simulated gamma lines to those of previously reported works [14-18, 37]. However, there are a few protons-induced prompt gamma spectrometer facilities that have been assembled in the world. We investigated the cross-section of produced prompt gamma rays versus proton energy and compared the results with those of experimental ones reported in the literature [18, 19, 37]. The results are in acceptable agreement between and show that the simulation of interactions and applied physics model are correct [19, 38]. In addition, we compared the simulated prompt gamma spectra of some elements with those of experimental ones in our previous work [38]. Furthermore, the validation of our study was accomplished according to the following steps:

1- Pre-defining a phantom and simulating the related spectrum.

2- Considering the simulated spectrum as the spectrum of an unknown phantom.

3- Analyzing the spectrum using the optimization methods.

4- Comparing the obtained weight percent of elements with those of pre-defined values.

3. Results

A set of library spectra from gamma lines of the ^{12}C, ^{16}O, ^{20}Ca, and ^{14}N elements in tissues, is established by simulating single-element phantoms with densities equivalent to test phantoms 1, 2, 3, and 4 reported in Table 1, respectively. The obtained gamma spectra due to the 30 MeV proton beam for ^{12}C, ^{20}Ca, ^{14}N, and ^{16}O elements with a density of phantom 3, with and without FWHM, are illustrated in Figures 2a, 2b, 2c, and 2d, respectively.

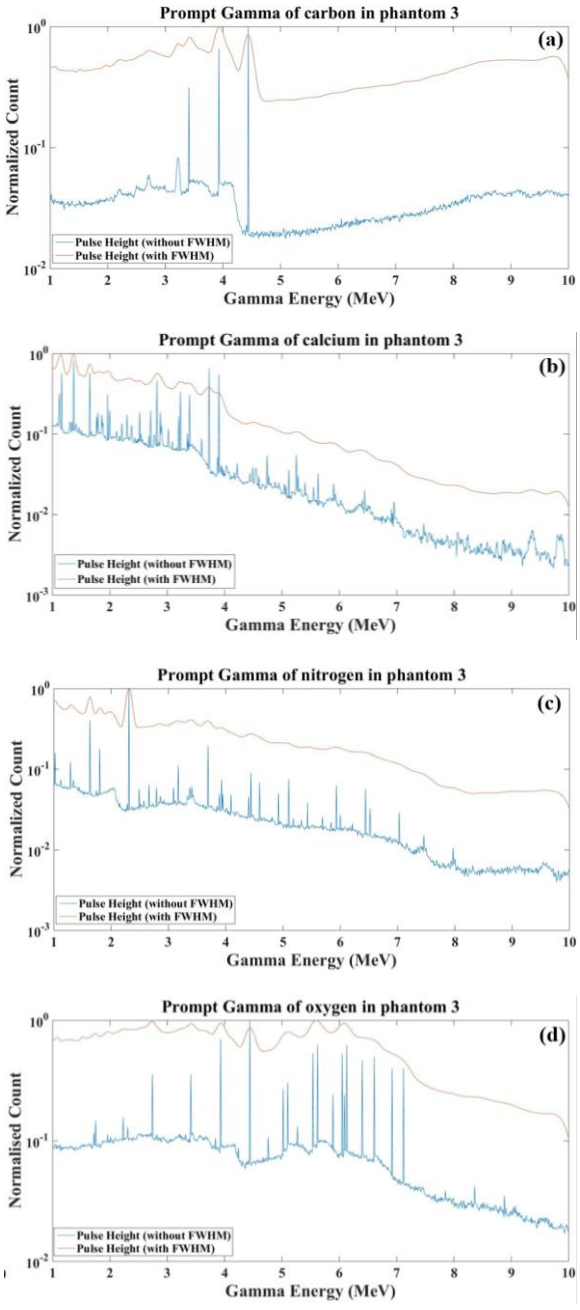

Figure 2. The library spectra of PG-ray for elements of phantom 3 corresponding to 30 MeV protons: (a) carbon, (b) calcium, (c) nitrogen, and (d) oxygen with and without FWHM broadening

To show detailed information on our considerations of physical interactions in simulations, a logarithmic plot of PG normalized counts before applying the detector FWHM related to part (a) of Figure 2 is presented in Figure 3. The PG lines, as well as the Compton continuum, Compton edge and single and double escape peaks (resulted from the pair production interaction) can be observed in the detector spectrum.

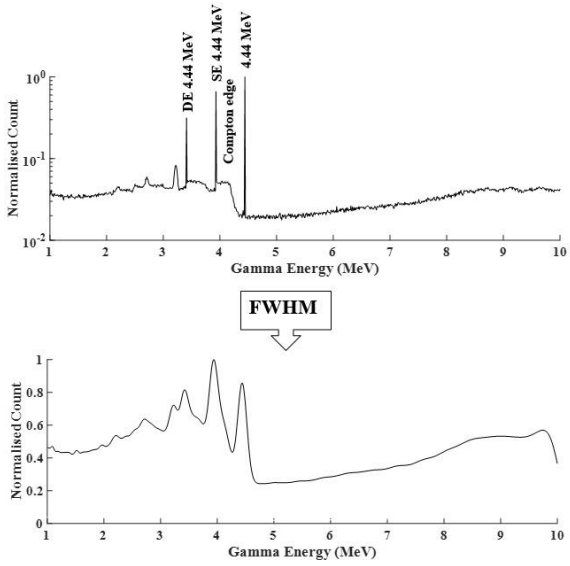

Figure 3. The PG-ray spectrum for the carbon of phantom 3 without (top panel) and with (bottom panel) FWHM broadening. The SE and DE in the upper part refer to single-scape and double-scape peaks

The proton history is 1e9 which is in order of clinical proton flux in the proton therapy. The mass concentration of elements is not directly from Monte Carlo simulations and the uncertainty of prompt gamma counts in each gamma energy-channel is low (as a quantitative scale, it is less than 0.1% in photo peaks of spectra). However, one of the advantages of WSA is its less sensitivity to low uncertainty of gamma counts in each channel.

The estimated quantities of each element (W_{est}) obtained from GA and MLR algorithms are listed in Tables 2, 3, 4, and 5 for 30 MeV protons corresponding to the phantoms 1, 2, 3, and 4, respectively. The nominal weights of each element in Table 1 are shown in the second column of these Tables. The Standard Deviations (STD), as a measure of precision, and the relative error, as a measure of accuracy, are also included in the Tables for both the GA and MLR methods.

In order to evaluate how well the GA and MLR algorithms can be used as a method to quantitatively estimate the elemental composition of a target from its

Table 2. Quantitative Elemental Analysis of phantom 1 corresponding to 30 MeV protons

Element	Nominal W (%)	MLR		GA	
		W_{est} ± STD (%)	Error (%)	W_{est} ± STD (%)	Error (%)
C	66.75	66.41 ± 0.57	0.50	66.50 ± 0.57	0.37
Ca	0	0	-	0	-
N	1.80	2.23 ± 0.24	23.71	2.05 ± 0.24	14.17
O	31.45	31.36 ± 0.28	0.28	31.44 ± 0.28	0.02

Table 3. Quantitative Elemental Analysis of phantom 2 corresponding to 30 MeV protons

Element	Nominal W (%)	MLR		GA	
		W_{est} ± STD (%)	Error (%)	W_{est} ± STD (%)	Error (%)
C	11.86	11.50 ± 0.60	3.03	11.66 ± 0.60	1.65
Ca	0	0	-	0	-
N	3.51	5.12 ± 0.26	45.85	4.93 ± 0.26	40.41
O	84.63	83.34 ± 0.30	1.48	83.41 ± 0.30	1.44

Table 4. Quantitative Elemental Analysis of phantom 3 corresponding to 30 MeV protons

Element	Nominal W (%)	MLR		GA	
		W_{est} ± STD (%)	Error (%)	W_{est} ± STD (%)	Error (%)
C	27.10	27.50 ± 0.61	1.47	27.69 ± 0.61	2.16
Ca	17.60	15.60 ± 0.11	11.39	15.60 ± 0.11	11.38
N	4.70	6.04 ± 0.26	28.59	5.99 ± 0.26	27.36
O	50.60	50.86 ± 0.30	0.51	50.73 ± 0.30	0.26

Table 5. Quantitative Elemental Analysis of phantom 4 related to 30 MeV protons

Element	Nominal W (%)	MLR		GA	
		W_{est} ± STD (%)	Error (%)	W_{est} ± STD (%)	Error (%)
C	16.12	16.15 ± 0.60	1.18	16.16 ± 0.60	0.26
Ca	0	0.23 ± 0.10	-	0.20 ± 10	-
N	3.84	3.73 ± 0.25	2.73	3.67 ± 0.25	4.34
O	80.04	79.89 ± 0.30	0.19	79.97 ± 0.30	0.09

gamma-ray spectra, the estimated weight (%) of each element is multiplied by the corresponding gamma-ray library spectrum to reversely construct the compound phantom gamma-ray spectrum. The reconstructed gamma-ray spectra corresponding to 30 MeV protons for GA and MLR methods and calculated spectra by Geant4 are shown in Figure 4 for test phantom 3. It has to be noted that similar results were obtained for reconstructed spectra related to phantoms 1, 2, and 4. For the sake of brevity, only the quantitative results are presented in Tables 2, 3, and 5.

To investigate the applicability of the proposed analysis method for higher energy protons, the elemental analysis was also performed for 70 and 150 MeV protons irradiated on phantom 3, as an example of our test phantoms. The analysis results corresponding to 70 MeV and 150 MeV protons for phantom 3 are presented in Tables 6 and 7, respectively. Furthermore, the reconstructed gamma-ray spectra for GA and MLR methods and calculated spectra using Geant4 corresponding to 70 MeV and 150 MeV are shown in Figures 5 and 6, respectively.

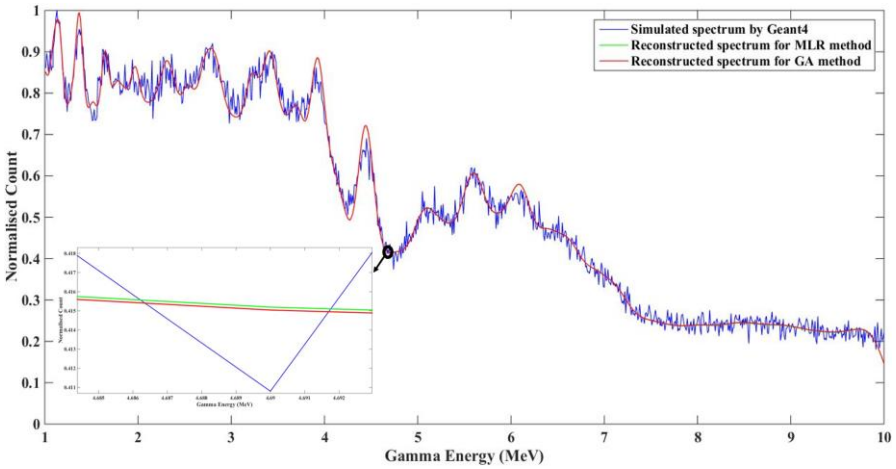

Figure 4. The reconstructed spectra obtained using MLR and GA methods and the calculated spectrum for phantom 3 corresponding to 30 MeV protons

Table 6. Quantitative Elemental Analysis of phantom 3 corresponding to 70 MeV protons

Element	Nominal W (%)	MLR		GA	
		W_{est} ± STD (%)	Error (%)	W_{est} ± STD (%)	Error (%)
C	27.10	26.64 ± 0.41	1.68	26.58 ± 0.41	1.92
Ca	17.60	17.16 ± 0.05	2.50	17.14 ± 0.05	2.58
N	4.70	6.06 ± 0.21	29.05	6.24 ± 0.21	32.84
O	50.60	50.13 ± 0.21	0.93	50.03 ± 0.21	1.12

Table 7. Quantitative Elemental Analysis of phantom 3 corresponding to 150 MeV protons

Element	Nominal W (%)	MLR		GA	
		W_{est} ± STD (%)	Error (%)	W_{est} ± STD (%)	Error (%)
C	27.10	22.88 ± 0.29	15.56	22.74 ± 0.29	16.09
Ca	17.60	17.31 ± 0.04	1.65	17.40 ± 0.04	1.15
N	4.70	8.57 ± 0.19	82.27	8.64 ± 0.19	83.78
O	50.60	51.24 ± 0.20	1.26	51.23 ± 0.20	1.24

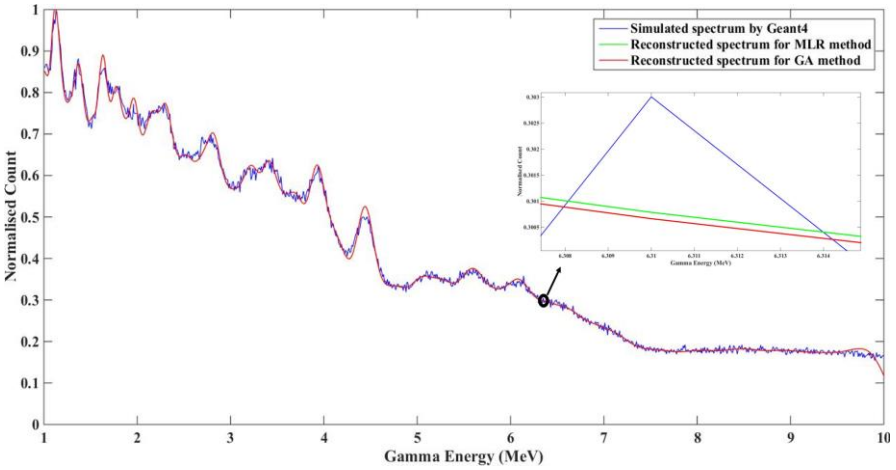

Figure 5. The reconstructed spectra obtained using MLR and GA methods and the calculated spectrum for phantom 3 corresponding to 70 MeV protons

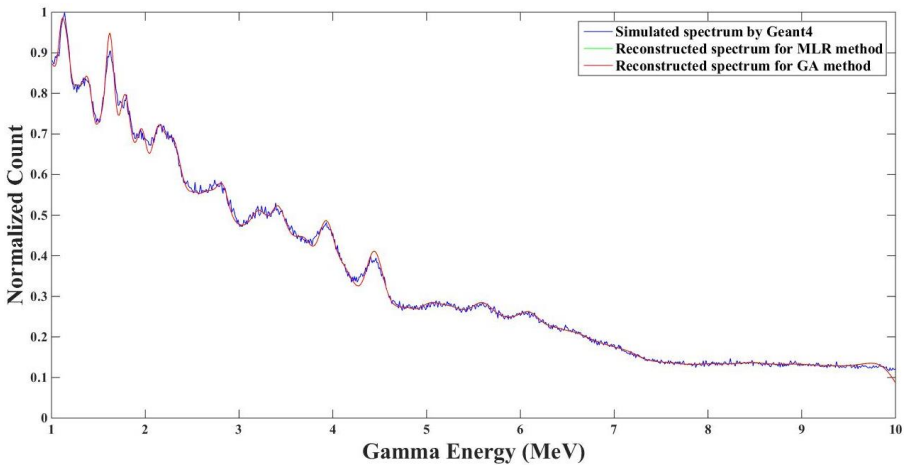

Figure 6. The reconstructed spectra obtained using MLR and GA methods and the calculated spectrum for phantom 3 corresponding to 150 MeV protons

To examine the effect of applying a detector shield and collimator on the analysis results, the 70 MeV protons and phantom 3 were selected as an example of considered proton energy and test phantom, respectively. The analysis results corresponding to this scenario are presented in Table 8. It should be noted that the present work is a preliminary study in this field aiming to investigate the effect of adding a collimator on improving the results. Optimizing the shield and collimator characteristics can be accomplished for a wider set of proton energies.

4. Discussion and Conclusion

The library spectra of the ^{12}C, ^{16}O, ^{20}Ca, and ^{14}N elements in human tissues studied in the current work include gamma lines of 4.44 MeV for carbon, 4.44, 6.13, 6.92, and 7.12 MeV for oxygen, 1.37, 3.74, and 3.91MeV for calcium, and 1.64, 2.32, and 5.11 MeV for nitrogen. According to the obtained results presented in Tables 2-5 for 30 MeV protons, Table 6 for 70 MeV protons, and Table 7 for 150 MeV protons, the weight percentage of oxygen is calculated accurately which is a vital piece clinical evidence for monitoring the cellular metabolism. The calculated weight percentage of carbon and calcium using both GA and MLR methods are in good agreement with the corresponding nominal values in all the test phantoms (Table 1), as shown in Tables 2-5 for 30 MeV protons, Table 6 for 70 MeV and Table 7 for 150 MeV protons. Generally, the relative errors of GA are smaller than those of MLR due to the applied cost function in the GA algorithm.

The main origin of relative errors in Tables 2-7 can be related to the statistical error. In addition, the lower counts of gamma lines are due to either small cross sections or a small amount of corresponding elements in the test phantoms. For example, since nitrogen is a minor element as shown in Table 1, the error related to the estimated concentration of nitrogen is larger than other elements according to the results presented in Tables 2-7. It should be noted that the smaller concentration of an element leads to its smaller contribution to the detector output spectrum and the estimated amount of that element is highly sensitive to the background. Furthermore, the estimated error of nitrogen concentration increases with increasing proton energy due to introducing more complexity to the spectra by generating similar peaks for different elements

Table 8. Quantitative Elemental Analysis of phantom 3 corresponding to 70 MeV protons for the collimated detector

Element	Nominal W (%)	MLR		GA	
		W_{est}±STD (%)	Error (%)	W_{est}±STD (%)	Error (%)
C	27.10	27.08±0.25	0.07	27.08±0.25	0.06
Ca	17.60	16.81±0.05	4.50	16.93±0.05	3.80
N	4.70	5.93±0.18	26.25	5.42 ± 0.18	15.42
O	50.60	50.18±0.16	0.83	50.56±0.17	0.08

such as 4.44 MeV gamma line for carbon, oxygen, and nitrogen. A significant improvement in estimating the nitrogen concentration can be seen by comparing the results presented in Tables 6 and 8 related to the uncollimated and collimated gamma-ray detector for 70 MeV protons, respectively. We think that the obtained results can be further improved by optimizing the different collimator characteristics.

In conclusion, the WSA approach was successfully applied to analyze the proton-induced PG-ray spectra obtained using 3 × 3 inch NaI(Tl) detectors. The required gamma-ray spectra were obtained using the Geant4 toolkit for single-element and multi-element phantoms. The results of applying the WSA in the obtained spectra of four test phantoms using the two well-known GA and MLR methods show that these methods provide an evaluation of the weight (%) of elements in different test phantoms. Strictly speaking, our analysis approach has the potential to be used for analyzing complex PG-ray spectra obtained using high-efficiency detectors (like NaI and BGO) in proton therapy setups.

This analysis method is useful for the online determination of the elemental composition of tissues near the Bragg peak in proton therapy. It determines the elemental composition of tissues from their measured PG-ray spectra along with Monte Carlo simulated library spectra. Moreover, it has the potential to be used for comparing the concentrations of elements in the normal and cancer tissues at different time points of the treatment period. However, more clinical considerations are required in simulation setups. The present study provides sufficient evidence for introducing a quantitative elemental analysis of proton-bombarded phantoms using their induced PG spectra.

References

1- Wayne D Newhauser and Rui Zhang, "The physics of proton therapy." *Physics in Medicine Biology*, Vol. 60 (No. 8), p. R155, (2015).

2- Harald Paganetti, "Range uncertainties in proton therapy and the role of Monte Carlo simulations." *Physics in Medicine and Biology*, Vol. 57 (No. 11), p. R99, (2012).

3- E Fiorina, INSIDE collaboration %J Nuclear Instruments, Spectrometers Methods in Physics Research Section A: Accelerators, Detectors, and Associated Equipment, "An integrated system for the online monitoring of particle therapy treatment accuracy." *Nuclear Instruments and Methods in Physics Research Section A: Accelerators, Spectrometers, Detectors and Associated Equipment*, Vol. 824pp. 198-201, (2016).

4- E Basile *et al.*, "An online proton beam monitor for cancer therapy based on ionization chambers with micro pattern readout." *Journal of Instrumentation*, Vol. 7 (No. 03), p. C03020, (2012).

5- Niccolo' Camarlinghi *et al.*, "An in-beam PET system for monitoring ion-beam therapy: test on phantoms using clinical 62 MeV protons." *Journal of Instrumentation*, Vol. 9 (No. 04), p. C04005, (2014).

6- S Muraro *et al.*, "Proton therapy treatment monitoring with the DoPET system: Activity range, positron emitters evaluation and comparison with Monte Carlo predictions." *Journal of Instrumentation*, Vol. 12 (No. 12), p. C12026, (2017).

7- Valeria Rosso *et al.*, "A new PET prototype for proton therapy: comparison of data and Monte Carlo simulations." *Journal of Instrumentation*, Vol. 8 (No. 03), p. C03021, (2013).

8- Metin Usta, Mustafa Çağatay Tufan, Güral Aydın, and Ahmet Bozkurt, "Stopping power and dose calculations with analytical and Monte Carlo methods for protons and prompt gamma range verification." *Nuclear instruments methods in physics research section A: Accelerators, Spectrometers, Detectors Associated Equipment*, Vol. 897pp. 106-13, (2018).

9- Veronica Ferrero *et al.*, "Evaluation of in-beam PET treatment verification in proton therapy with different reconstruction methods." *IEEE Transactions on Radiation and Plasma Medical Sciences*, Vol. 4 (No. 2), pp. 202-11, (2019).

10- J Krimmer, D Dauvergne, JM Létang, and É Testa, "Prompt-gamma monitoring in hadrontherapy: A review." *Nuclear Instruments and Methods in Physics Research Section A: Accelerators, Spectrometers, Detectors and Associated Equipment*, Vol. 878pp. 58-73, (2018).

11- F Stichelbaut and Y Jongen, "Verification of the proton beam position in the patient by the detection of prompt gamma-rays emission." in *39th PTCOG meeting, San Francisco*, (2003).

12- Chul-Hee Min, Chan Hyeong Kim, Min-Young Youn, and Jong-Won Kim, "Prompt gamma measurements for locating the dose falloff region in the proton therapy." *J Applied physics letters*, Vol. 89 (No. 18), p. 183517, (2006).

13- E Testa *et al.*, "Monitoring the Bragg peak location of 73 MeV⁄ u carbon ions by means of prompt γ-ray measurements." *J Applied physics letters*, Vol. 93 (No. 9), p. 093506, (2008).

14- J Polf, S Peterson, G Ciangaru, M Gillin, and S Beddar, "Prompt gamma-ray emission from biological tissues during proton irradiation: a preliminary study." *J Physics in Medicine Biology*, Vol. 54 (No. 3), p. 731, (2009).

15- J Polf *et al.*, "Measurement and calculation of characteristic prompt gamma ray spectra emitted during proton irradiation." *J Physics in Medicine Biology,* Vol. 54 (No. 22), p. N519, (2009).

16- Jerimy Polf *et al.*, "Measurement of characteristic prompt gamma rays emitted from oxygen and carbon in tissue-equivalent samples during proton beam irradiation." *J Physics in Medicine Biology,* Vol. 58 (No. 17), p. 5821, (2013).

17- Joost M Verburg and Joao Seco, "Proton range verification through prompt gamma-ray spectroscopy." *J Physics in Medicine Biology,* Vol. 59 (No. 23), p. 7089, (2014).

18- Joost M Verburg, Helen A Shih, and Joao Seco, "Simulation of prompt gamma-ray emission during proton radiotherapy." *J Physics in Medicine Biology,* Vol. 57 (No. 17), p. 5459, (2012).

19- Fereshte Saheli *et al.*, "Single peak analysis of proton induced prompt gamma counts." *Nuclear Instruments and Methods in Physics Research B,* Vol. 475pp. 63-70, (2020).

20- Robin P Gardner, A Sood, YY Wang, L Liu, P Guo, and RJ Gehrke, "Single peak versus library least-squares analysis methods for the PGNAA analysis of vitrified waste." *J Applied radiation isotopes,* Vol. 48 (No. 10-12), pp. 1331-35, (1997).

21- Miltiadis Alamaniotis and Tatjana Jevremovic, "Hybrid fuzzy-genetic approach integrating peak identification and spectrum fitting for complex gamma-ray spectra analysis." *J IEEE Transactions on Nuclear Science,* Vol. 62 (No. 3), pp. 1262-77, (2015).

22- L Salmon, "Analysis of gamma-ray scintillation spectra by the method of least squares." *J Nuclear Instruments Methods in Physics Research Section B: Beam Interactions with Materials Atoms,* Vol. 14pp. 193-99, (1961).

23- Marica Baldoncini *et al.*, "Investigating the potentialities of Monte Carlo simulation for assessing soil water content via proximal gamma-ray spectroscopy." *J Journal of environmental radioactivity,* Vol. 192pp. 105-16, (2018).

24- Sea Agostinelli *et al.*, "GEANT4—a simulation toolkit." *J Nuclear Instruments Methods in Physics Research Section A: Accelerators, Spectrometers, Detectors Associated Equipment,* Vol. 506 (No. 3), pp. 250-303, (2003).

25- H Shahabinejad and SAH Feghhi, "Design, optimization and performance of source and detector collimators for gamma-ray scanning of a lab-scale distillation column." *Applied Radiation and Isotopes,* Vol. 99pp. 25-34, (2015).

26- John Furey and Cliff Morgan, "Quartic collimator design for high-energy gamma rays." *Nuclear Instruments and Methods in Physics Research Section B: Beam Interactions with Materials and Atoms,* Vol. 629 (No. 1), pp. 202-05, (2011).

27- Zanyar Movasaghi, Shazza Rehman, and Dr Ihtesham Jur Rehman, "Fourier transform infrared (FTIR) spectroscopy of biological tissues.", *Applied Spectroscopy Reviews,* Vol. 43 (No. 2), pp. 134-79, (2008).

28- Hashem Miri Hakimabad, Hamed Panjeh, and Alireza Vejdani-Noghreiyan, "Evaluation the nonlinear response function of a 3× 3 in NaI scintillation detector for PGNAA applications." *J Applied radiation isotopes,* Vol. 65 (No. 8), pp. 918-26, (2007).

29- Ilker Meric, Geir A Johansen, Marie B Holstad, Jiaxin Wang, and Robin P Gardner, "Produced water characterization by prompt gamma-ray neutron activation analysis." *J Measurement Science Technology,* Vol. 22 (No. 12), p. 125701, (2011).

30- Hadi Shahabinejad and Naser Vosoughi, "SGSD: A novel Sequential Gamma-ray Spectrum Deconvolution algorithm." *Annals of Nuclear Energy,* Vol. 132pp. 369-80, (2019).

31- Hadi Shahabinejad and Naser Vosoughi, "Analysis of complex gamma-ray spectra using particle swarm optimization." *J Nuclear Instruments Methods in Physics Research Section A: Accelerators, Spectrometers, Detectors Associated Equipment,* Vol. 911pp. 123-30, (2018).

32- David E Goldberg, "Genetic algorithm." *J Search, Optimization Machine Learning,* pp. 343-49, (1989).

33- John Holland, "Adaptation in natural and artificial systems: an introductory analysis with application to biology." *J Control artificial intelligence,* (1975).

34- H Shahabinejad, SA Hosseini, and M Sohrabpour, "A new neutron energy spectrum unfolding code using a two steps genetic algorithm." *J Nuclear Instruments Methods in Physics Research Section A: Accelerators, Spectrometers, Detectors Associated Equipment,* Vol. 811pp. 82-93, (2016).

35- Vitisha Suman and PK Sarkar, "Neutron spectrum unfolding using genetic algorithm in a Monte Carlo simulation." *J Nuclear Instruments Methods in Physics Research Section A: Accelerators, Spectrometers, Detectors, Associated Equipment,* Vol. 737pp. 76-86, (2014).

36- Miltiadis Alamaniotis, John Mattingly, and Lefteri H Tsoukalas, "Pareto-Optimal gamma spectroscopic radionuclide identification using evolutionary computing." *J IEEE Transactions on Nuclear Science,* Vol. 60 (No. 3), pp. 2222-31, (2013).

37- Jeyasingam Peterson Jeyasugiththan, Stephen W, "Evaluation of proton inelastic reaction models in Geant4 for prompt gamma production during proton radiotherapy." in *J Physics in Medicine Biology* Vol. 60, ed, (2015), p. 7617.

38- F Saheli, Z Riazi, A Jokar, H Shahabinejad, N Vosoughi, and SA Ghasemi, "Evaluation the nonlinear response function of a HPGe detector for 59 keV to 10.7 MeV gamma-rays using a Monte Carlo simulation and comparison with experimental data.", *Journal of Instrumentation,* Vol. 16 (No. 07), p. P07003, (2021).